Hindawi
Advances in Civil Engineering
Volume 2022, Article ID 3465281, 12 pages
https://doi.org/10.1155/2022/3465281

Research Article

Study on Mechanical Behavior of Reinforced Concrete Beams under Sulfate Attack

Xiaomeng Zang,[1] **Genhui Wang**,[1] **Zichen Zhang**,[1] **Xiaolu Duan**,[2] **and Xiaoying Hu**[3]

[1]*School of Civil Engineering, Lanzhou Jiaotong University, Lanzhou, Gansu 730070, China*
[2]*China Railway Eryuan Engineering Group Co. Ltd., Chengdu, Sichuan 610031, China*
[3]*School of Civil Engineering, Lanzhou University of Technology, Lanzhou, Gansu 730050, China*

Correspondence should be addressed to Xiaomeng Zang; zangxm@lzjtu.edu.cn

Received 23 December 2021; Revised 10 February 2022; Accepted 5 April 2022; Published 22 April 2022

Academic Editor: Yonghong Wang

In order to analyze the influence of sulfate corrosion on the mechanical behavior of reinforced concrete beams, the dry-wet cyclic corrosion test was carried out on the model test beams, and the two test beams corroded for 0 d and 60 d were statically loaded, respectively. Then, the changes in flexural mechanical properties of the two test beams corroded for 0 d and 60 d were studied. Finally, the nonlinear finite element model was created by using ABAQUS. The plastic damage model is used to reflect the sulfate corrosion, and the mechanical properties of concrete beams under long-term sulfate corrosion are further analyzed. The results show that the compressive strength of the test beam concrete after 60 days of corrosion is 13.6% higher than that before corrosion, which indicates that the strength of concrete is increased by sulfate corrosion in the early stage. With the increase of sulfate corrosion time, the strength and stiffness of the beam first increase and then decrease. With the change in corrosion time, the cracking load and flexural capacity first increase and then decrease, which is consistent with the mechanism of sulfate densification first and then deterioration of the concrete structure. The calculation formulas of cracking load and bending capacity obtained by fitting are accurate.

1. Introduction

A large number of salt lakes and saline soils are distributed in Northwest China. Salt corrosion caused by these special geographical environments is very common. Due to salt corrosion, many reinforced concrete structures appear diseased and even structural failure may result in advance, which seriously affects the service life of the structure. Among the salt corrosion problems, sulfate corrosion is particularly prominent and needs to be paid attention to. Common sulfate corrosion mainly occurs in industrial buildings (such as chemical plants), underground buildings, coastal buildings, highway and railway facilities in saline soil environment, and hydraulic structures in inland salt lakes. For concrete bridges, not only the foundation pier but also the upper beam body has been seriously corroded by sulfate [1–8]. With the rapid development of the world, China's various highways, railways, and other infrastructures are under vigorous construction, which puts forward higher requirements for the safety and durability of concrete structures. Therefore, it is necessary to study the stress of concrete structures in a sulfate corrosion environment [9, 10]. Nowadays, the research on sulfate corrosion is mostly focused on the level of concrete materials, such as the weight change rate of concrete test block with corrosion time and the change of dynamic elastic modulus and compressive strength [11–15]. However, and there are relatively few studies on the degradation of mechanical properties of concrete beams under sulfate corrosion. It is necessary to combine the existing research results in materials and further explore the content of the research structure level on this basis. At the same time, the specifications and test conditions are limited, and the indoor test is difficult to match the engineering practice, so a more perfect test

scheme needs to be designed [9]; for example, test beam size design, section reinforcement design, test solution configuration, mechanical test scheme, and other specific operation processes need to be further refined.

Based on the existing research, this paper designs the sulfate immersion test of reinforced concrete beam model and compares and analyzes the influence of sulfate corrosion on the mechanical properties of reinforced concrete box girder through static loading test, and the finite element model is established by using ABAQUS nonlinear analysis software [16–25] and reflects the sulfate corrosion by changing the relevant parameters in the plastic damage model. Then, the finite element calculation results are compared with the test results. The change in flexural mechanical properties of the test beam under long-term sulfate corrosion is analyzed by using the finite element model. Finally, the deterioration model of cracking load, flexural bearing capacity with corrosion time, and the degradation of the flexural effective section are obtained. Therefore, it has a certain guiding significance for the prediction of bearing capacity and service life of concrete bridges under similar corrosion conditions.

2. Test Overview

2.1. Test Purpose. In this paper, through experimental research the components were immersed in a 10% Na_2SO_4 solution. In order to speed up the corrosion process, the test was carried out in a dry-wet cycle mode close to the test conditions described in reference [26]. After that, the beams with corrosion time of 0 d and 60 d were tested by static loading failure mechanics. The whole test process is recorded, the test results are analyzed, and the changes in flexural mechanical properties of the two are compared, so as to provide an effective method and means for the study of the mechanical behavior of reinforced concrete beams under sulfate attack.

2.2. Test Scheme

2.2.1. Fabrication of Test Piece. The test beam with box section is designed for the sulfate corrosion test. The length of the test beam is $L = 2000$ mm, the concrete grade is C40, and the shear span ratio is 2.74. An embedded steel plate is set at the left and right of the bottom of the beam to prevent local concrete from being damaged under the action of concentrated force. The section size and reinforcement are shown in Figure 1, and the longitudinal reinforcement adopts Φ_6 ribbed reinforcement and stirrup Φ_6 ribbed reinforcement.

2.2.2. Layout of Measuring Points and Data Acquisition. The concrete strain gauge has been pasted at the midspan section of the test beam, with a resistance value of $120.5 \pm 0.2\%$ and a sensitivity coefficient of $2.032 \pm 0.26\%$ (the strain gauge has been pasted at the reinforcement of the midspan section before pouring concrete). The pasting position and the corresponding serial number of the concrete and reinforcement strain gauge are shown in Figure 2. Two dial indicators of model YHD-100 with a measuring range of 0~30 mm and an accuracy of 0.01 mm are symmetrically installed on the midspan bottom surface of the beam body to measure the midspan displacement of the test beam $f_0 = (f_1 + f_2)/2$. At the same time, the same dial indicators are arranged at the supports at both ends of the beam to measure the settlement f_3 and f_4 of the supports and then the midspan deflection of the beam $f = (f_1 + f_2)/2 - (f_3 + f_4)/2$.

2.2.3. Immersion Model Beam. The beam body cured for 28 d and reaching the corresponding concrete strength shall be placed in a pool with a length of 2.2 m, a width of 1.4 m, and a height of 0.7 m. Pour the prepared 10% sodium sulfate solution into the tank and completely soak the beam. The dry-wet cycle period is 15 days, the sodium sulfate solution is soaked for 7 days, and then the solution in the tank is pumped dry and dried at room temperature for 8 days [27–29], as shown in Figure 3.

2.2.4. Loading of Model Beam. Four-point bending static loading failure tests were carried out on the test beams corroded for 0 d and 60 d, respectively, to study their flexural mechanical properties. The beam numbers are 0 beam and 1 beam, respectively (both beams are cured in the same batch and under the same conditions). The two concentrated forces act on one-third of the beam span. The source of the force is the hydraulic jack, which is distributed through a distribution beam. Step-by-step loading is adopted, and each level stays for 5~10 minutes to obtain a stable measured value. The loading device is shown in Figure 4.

3. Analysis of Test Results

During the loading process of the No. 0 test beam, when the load reaches 24 kN, the first small crack appears at the midspan at the bottom of the beam, with a width of about 0.1 mm, which is regarded as the cracking load, which is close to the theoretical cracking load of 25 kN. With the increasing load, the crack in the middle of the span continues to develop, and then, the inclined crack also occurs in the support, and then, the crack extends upward along the beam height direction. When the load reaches about the yield load, the width of the inclined crack increases obviously; for example, one of the cracks increases from 1 mm to about 2 mm. Some different cracks are connected together to form the main crack, which continuously extends to the beam top, and the average spacing of cracks is 100 mm. With the continuous application of load, when the load reaches 170 kN, it is difficult to apply the load, the load cannot be applied continuously, and there is a gradual downward trend. The deflection in the middle of the span increases rapidly, and the maximum deflection is 3.284 mm. Finally, the concrete in the shear compression zone is damaged, the maximum crack width reaches about 2.5 mm, and the structure fails.

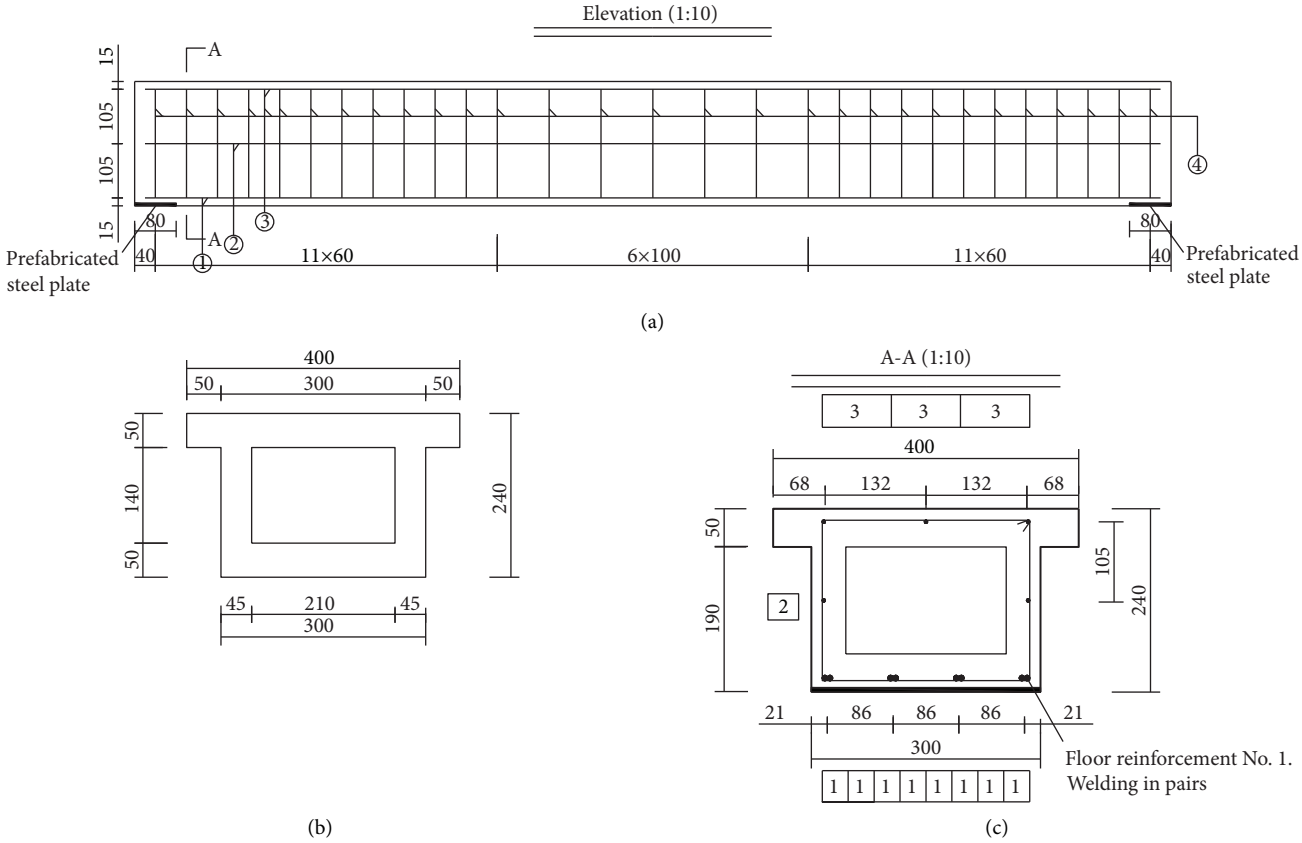

Figure 1: Section size and reinforcement arrangement of test beam (unit: mm). (a) Elevation. (b) Section. (c) Reinforcement layout.

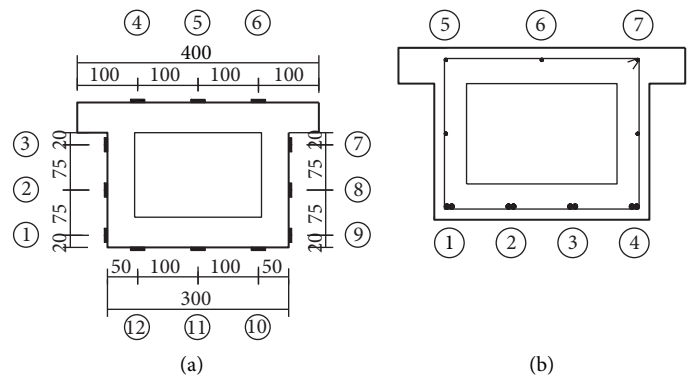

Figure 2: Arrangement of strain gauge of test beam (unit: mm). (a) Arrangement of concrete strain gauges. (b) Arrangement of reinforcement strain gauge.

The rebound value of the No. 1 test beam is measured before and after corrosion, and the change of concrete compressive strength can be obtained by correcting its carbonation depth. Through comparison, it can be found that the concrete compressive strength after 60 days of corrosion is 13.6% higher than that before corrosion, indicating that the concrete compressive strength of the beam body will be improved to a certain extent in the early stage of sulfate corrosion concrete beam. However, due to the short corrosion time, the mechanical test results are only slightly different from those in the noncorroded state. The situation of the whole test process is basically the same as that of the corroded 0 d test beam. When the first crack appears, the loading force is 32 kN, and the crack width is about 0.1 mm. With the continuous increase of the load, the crack at the middle of the span continues to develop, and then, the support also produces oblique cracks. The cracks extend upward in the beam height direction, the vertical cracks and oblique cracks continue to increase, the crack width also gradually increases, and the average spacing of cracks is 105 mm. When the loading force reaches 170 kN, the test beam is still under normal stress. After that, the force

(a) (b)

Figure 3: Immersion test of the model beam. (a) Immersion model beam. (b) 10% Na_2SO_4 solution configuration.

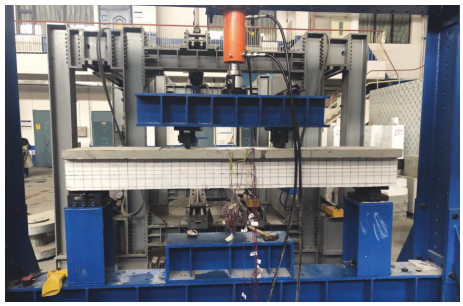

Figure 4: Loading device diagram.

continues to increase, and the deflection continues to increase. When it reaches a certain degree, the force cannot continue to be applied, it is unloaded automatically, the concrete at the inclined section is crushed, the structure fails and destroys, the test beam is damaged by bending, and the crack distribution is shown in Figure 5.

The cracking load is obtained through the test, and the change of yield load is shown in Table 1. The yield load of the test beam is controlled by the yield stress of the tensile reinforcement at the bottom [30, 31].

It can be seen from Table 1 that the cracking load of the current test beam increases with the change of corrosion days; that is, the cracking load of the 60-day corrosion test beam is increased by 33.3% compared with that before corrosion. The reason for this is that the corrosion degree will have a certain impact on the cracking load of the beam. At the initial stage of corrosion, sulfate will react with the concrete to produce expansive products, which will continuously compact the concrete, so as to enhance the crack resistance of the concrete. On the other hand, the expansive products will produce expansive internal stress in the concrete. When the concrete is under load, it is necessary to offset this part of the stress before the concrete is tensioned, so the cracking load increases. Similarly, the yield load of the test beam corroded for 60 days also increases by 3%.

4. Finite Element Model of Structure

4.1. Plastic Damage Model of Concrete. The concrete strength index reduction method is adopted to consider the impact of sulfate immersion corrosion on concrete strength. In ABAQUS software, the plastic damage model is a model based on plastic continuum damage. The principle is to use the combination of isotropic damage elasticity, isotropic tension, and compression plasticity to reflect the inelastic behavior of concrete [32]. In this paper, the plastic damage model is used to study the change of flexural mechanical properties of the test beam with the corrosion time, ignoring the factors such as the corrosion of reinforcement caused by sulfate corrosion and the change of bonding force between reinforcement and concrete [33, 34].

The key of the plastic damage model is to obtain the parameters of concrete CDP (concrete damaged plastic) constitutive relationship corresponding to different corrosion times to reflect the sulfate corrosion. The stress-strain curves of concrete are mainly divided into two types: one is the full stress-strain curve under uniaxial compression and the other is the full stress-strain curve under uniaxial tension.

Through the formula in references [35–37], the eigenvalue reflecting the constitutive relationship of concrete after corrosion can be calculated.

4.1.1. Constitutive Relation of Uniaxial Compression. According to the characteristics of the stress-strain curve of concrete under axial compression, document [36] proposed a curve equation with a cubic polynomial in the rising section and rational formula in the falling section, namely,

$$y = \begin{cases} ax + (3-2a)x^2 + (a-2)x^3, & 0 \le x \le 1, \\ \dfrac{x}{b(x-1)^2 + x}, & x \ge 1, \end{cases} \quad (1)$$

where $x = \varepsilon/\varepsilon_{pr}$, $y = \sigma/\sigma_{pr}$: ε_{pr} is the peak strain of concrete; σ_{pr} is the peak stress of concrete; and a, b are the parameters of rising section and falling section related to materials, respectively.

4.1.2. Constitutive Relation of Uniaxial Tension. According to reference [36], the full tensile stress-strain curve can also be described by a two-stage formula, that is, rising

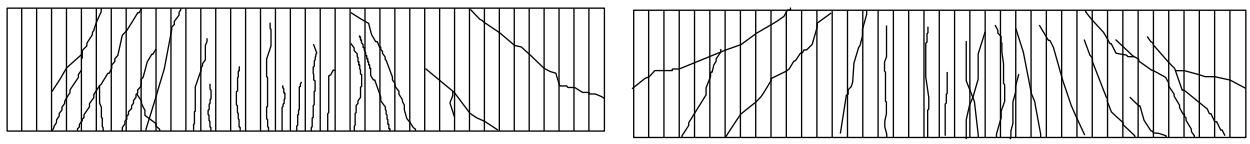

(a) (b)

Figure 5: Fracture correlation. (a) Crack distribution in the web of No. 0 test beam. (b) Crack distribution in the web of No. 1 test beam.

Table 1: Test results of cracking load and yield load of test beam.

Number of test beam	Cracking load (kN)	Cracking moment M_{cr} (kN·m)	M_{cr}/M_{cr0}	Yield load (kN)	Yield moment M_y (kN·m)	M_y/M_{y0}
No. 0 test beam	24	8	1	149	49.67	1
No. 1 test beam	32	10.67	1.33	154	51.33	1.03

Note: M_{cr} is the cracking moment of the test beam corroded by sulfate; M_{cr0} is the cracking moment of the test beam not corroded by sulfate; M_y is the yield moment of the test beam corroded by sulfate; and M_{y0} is the yield moment of the test beam not corroded by sulfate.

stage and falling stage. The specific expression is as follows:

$$y = \begin{cases} 1.2x - 0.2x^6, & x \le 1, \\ \dfrac{x}{a_t (x-1)^{1.7} + x}, & x \ge 1. \end{cases} \quad (2)$$

The initial parameters of axial compressive strength are obtained by measuring the cube compressive strength of concrete test blocks with the same batch and strength grade of 100 mm × 100 mm × 100 mm as the test beam and multiplying the corresponding coefficient. The size is 34.1 MPa. Other parameters such as expansion angle 38, eccentricity 0.1, $f_{b0}/f_{c0} = 1.16$, $k = 0.66667$, viscosity parameter 0.05 are selected. The eigenvalues of concrete constitutive relationships corresponding to different corrosion times are shown in Table 2.

By analyzing the data in the table, it can be seen that the variation of each characteristic value of concrete is similar, which increases first and then decreases gradually. By using the relevant calculation tables and inputting the above parameters, the corresponding CDP constitutive relationship can be obtained. The stress-strain curves of concrete test blocks corroded for 0 d, 120 d, 360 d, and 600 d are compared, and the results are shown in Figure 6.

As can be seen from Figure 6, the height of the curve position is ranked as 120 d, 0 d, 360 d, and 600 d, indicating that the compressive stress-strain curve and tensile stress-strain curve belong to an upward trend from 0 to 120 d, and there is an overall downward trend after 120 d, with a greater degree of decline and a faster rate of decline. It shows that the performance of concrete changes with the corrosion time. In the early stage, the corrosion degree of sulfate on concrete is relatively light and even improves its strength to a certain extent. Then, the overall trend is decreased, and the deterioration speed is gradually accelerated, which has a serious impact on the performance of concrete and accelerates the deterioration of overall strength.

4.2. Numerical Analysis Model

4.2.1. Element Selection. The material properties of reinforcement and concrete are quite different. When dividing the calculation unit of the structure, according to the different methods of dealing with the two materials, three methods can be adopted: integral model, separated model, and combined element model [36]. The separated model divides reinforcement and concrete into different types of elements and gives different material parameters.

The characteristic modeling method [38] is used to establish the numerical analysis model of the reinforced concrete beam. The model size and reinforcement layout are consistent with the test concrete beam shown in Figure 1. The concrete adopts an eight-node hexahedral isoparametric element (C3D8) with reduced integral, and the reinforcement adopts a two-node three-dimensional linear truss element (T3D2). The reinforcement cage is built into the concrete by using the method of a built-in unit [39, 40].

4.2.2. Analysis Method and Convergence Criterion. Solid structure analysis is to solve the structural state response quantity that satisfies three kinds of basic equations under external action under given boundary conditions and initial conditions, including stress, strain, and displacement. Implicit algorithm or explicit algorithm can be used to solve the nonlinear equations of reinforced concrete structures. Among them, the implicit algorithm adopts the Newton–Raphson method to solve the nonlinear equation. In the process of solving, it is necessary to inverse the stiffness matrix at the current time.

4.2.3. Loads and Boundary Conditions. Mutual restraint is established between the reinforcement to form a whole, and the three-point loading is carried out on the model according to the test operation. The reference point RP-1 and the loading area are set, as shown in Figure 7. The two are coupled and connected, and then, the load is applied to

Table 2: Constitutive parameters of concrete corresponding to corrosion days.

Days of corrosion (d)	Axial compressive strength (MPa)	Compressive peak strain ($\mu\varepsilon$)	Elastic modulus (MPa)	Tensile strength (MPa)	Tensile peak strain ($\mu\varepsilon$)
0	34.1	1704	34555	3.17	121
60	34.6	1712	34697	3.20	122
120	34.6	1712	34701	3.20	122
240	33.1	1690	34286	3.11	120
360	29.6	1635	33268	2.88	115
480	24.0	1542	31526	2.51	107
600	16.3	1395	28782	1.94	93

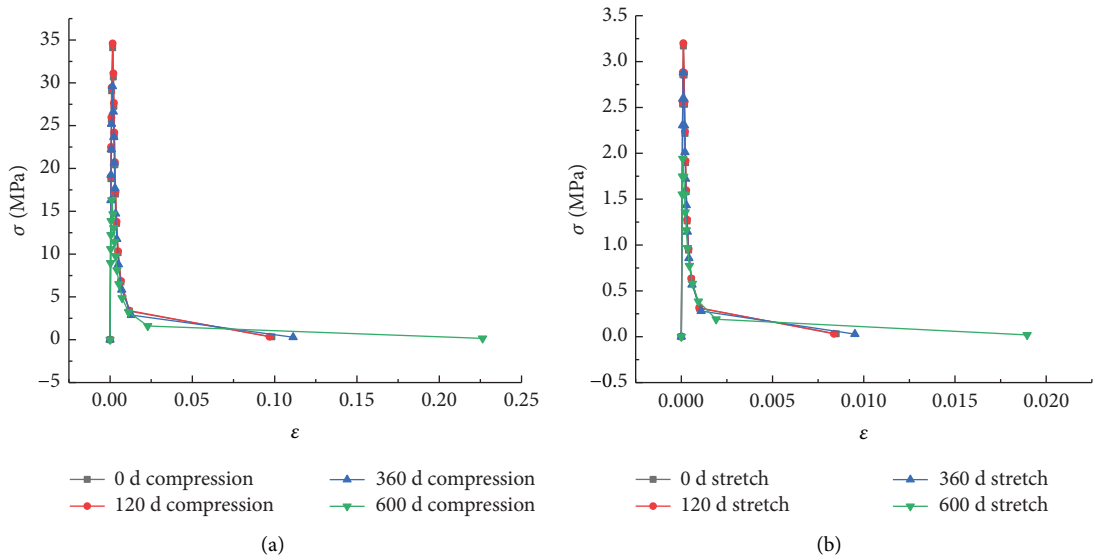

Figure 6: Comparison of stress-strain curves of concrete under different corrosion days. (a) Compressive stress-strain curve of the concrete test block. (b) Tensile stress-strain curve of the concrete test block.

the reference point to avoid stress concentration. The load is applied to the reference point RP-1, and then, the boundary conditions are created according to the simply supported structure.

4.2.4. Contact Conditions. Reinforcement and concrete are set in built-in contact.

4.3. Type of Element and Verification of Mesh Sensitivity. ABAQUS software sets up a rich element library to meet the requirements of different problems for different element types. At present, the commonly used element types in the structural analysis of solid materials include truss element (rod element), beam element, solid element, shell element, rigid body element, and membrane element. In this paper, the concrete adopts a spatial solid element, and the reinforcement adopts a spatial truss element.

Considering that the displacement mode [38] of the spatial 4-node tetrahedral element is a linear function similar to the plane 3-node triangular element, and the strain matrix of each element is constant, and its accuracy is often poor [41]. In this study, the concrete adopts the spatial 8-node hexahedron element, and the reinforcement adopts the

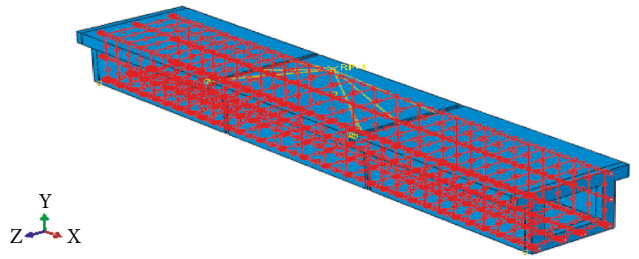

Figure 7: Interaction diagram.

spatial 2-node truss element. The 8-node hexahedron element adopts the displacement mode with three mixed quadratic terms and one mixed cubic term. The maximum number of times of its strain matrix is 2, which can accurately simulate the deformation of the element. Therefore, the spatial 8-node hexahedron element can be used to simulate the strain of the model concrete material.

In order to analyze the influence of element size on the calculation results of the concrete beam, the maximum Mises stress and S33 stress of concrete beam under 6 mm displacement loading are compared and analyzed by using different mesh sizes. The results are listed in Table 3. The

Table 3: Influence of element and mesh size on analysis results.

Mesh scheme	Concrete		Rebar		Mises stress (MPa)
	Element type	Grid size (mm)	Element type	Grid size (mm)	
Mesh 1	C3D8R	25	T3D2	25	6.15
Mesh 2	C3D8R	12.5	T3D2	12.5	9.1
Mesh 3	C3D8R	10.0	T3D2	10.0	10.2
Mesh 4	C3D8R	7.5	T3D2	7.5	10.3
Mesh 5	C3D20R	10.0	T3D3	10.0	10.2

analysis results show that when the concrete element is 10 mm and the reinforcement element is 10 mm, the influence of refining the element size on the analysis results is gentle.

In this paper, the numerical simulation of reinforced concrete beams is carried out by using reinforcement and concrete elements with an approximate size of 10 mm. The box section concrete beam is divided into 55440 spatial 8-node hexahedral reduced integral elements, and the reinforcement skeleton is divided into 2052 spatial 2-node linear truss elements.

4.4. Comparison between Numerical Simulation and Model Test Results. By using ABAQUS software, the nonlinear finite element models under seven corrosion conditions are established. The corrosion days are 0 d, 60 d, 120 d, 240 d, 360 d, 480 d, and 600 d, respectively. Now, the corrosion 0 d model is taken as an example. The whole tensile damage nephogram can reflect the location and development process of cracks. Figure 8 shows the tensile damage in the last frame of the ABAQUS model, and Figure 8 shows the midspan deflection nephogram of the ABAQUS model test beam.

It can be seen from Figure 8 that there is serious tensile damage in the lower midspan of the test beam and its adjacent areas, and there is a tensile stress concentration area at the concentrated loading point, which is consistent with the above mechanical test phenomena. It can be seen from Figure 9 that when the load is 170 kN, the deflection of the middle span of the test beam is large, and the maximum value is at the middle of the span, which is 3.328 mm, which is 1.3% different from the test result of 3.284 mm, indicating that the ABAQUS model is in good agreement with the test.

4.4.1. Load Strain Analysis. The load strain comparison of the concrete at the bottom of the model test beam is shown in Figure 10. It can be seen from Figure 10 that the change trend of corrosion 0 d test value and finite element calculation value is basically the same, and the difference between values is small. Similarly, the fitting degree between the load strain test value of concrete corroded for 60 days and the results of the finite element model is also high, which shows that the test results are reliable, and the method of nonlinear simulation analysis of test beam by using ABAQUS plastic damage model is effective.

4.4.2. Long-Term Sulfate Corrosion. In the previous step, the feasibility of ABAQUS nonlinear simulation is verified. Therefore, with the help of the nonlinear analysis finite element model, the change of flexural mechanical properties of concrete beams under long-term corrosion can be studied, and the load-strain curve corresponding to each corrosion day can be obtained, as shown in Figure 11.

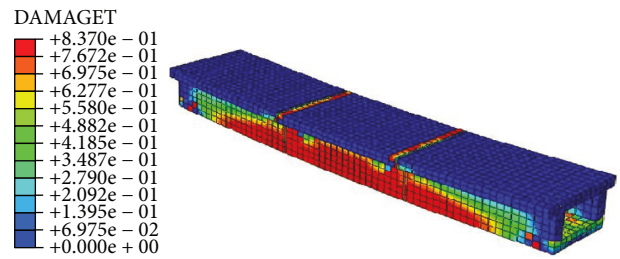

Figure 8: Nephogram of tensile damage of test beam.

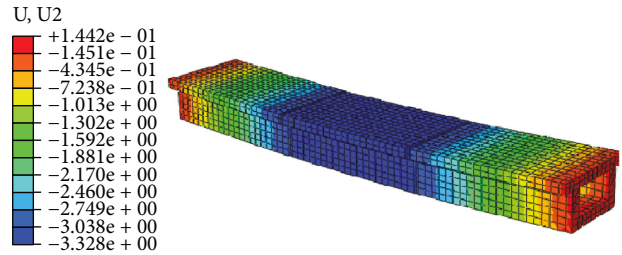

Figure 9: Nephogram of midspan deflection of test beam.

It can be seen from Figure 11 that when the load is small, the concrete strain corresponding to different corrosion times is basically the same or the difference is very small. When the action load is increased, the concrete strain of each corrosion beam is significantly different. The longer the corrosion time is, the greater the concrete strain under the same load, and the maximum increase is about 42%. At this time, the influence on the mechanical properties of the whole structure is obvious. When the load continues to increase to a certain extent, the difference gradually decreases, and the concrete strain value under each corrosion condition is almost equal. On the whole, long-term sulfate corrosion will increase the strain of concrete and reduce the flexural mechanical properties of test beams.

4.4.3. Analysis of Load Deflection Curve of Test Beam. The load-displacement curve corresponding to each corrosion day is obtained by ABAQUS finite element model, as shown in Figure 12.

It can be seen from Figure 12 that with the increase of sulfate corrosion time, the overall curve deviates to the lower

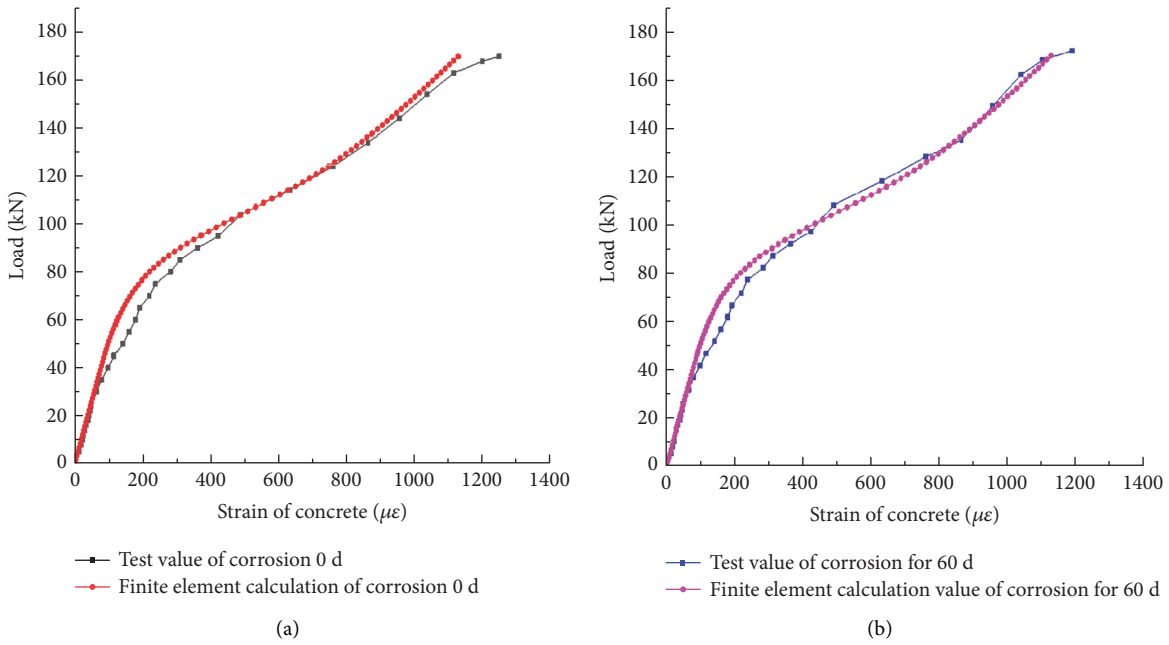

Figure 10: Load strain diagram of beam bottom concrete. (a) Load strain diagram of corrosion 0 d. (b) Load strain diagram of corrosion 60 d.

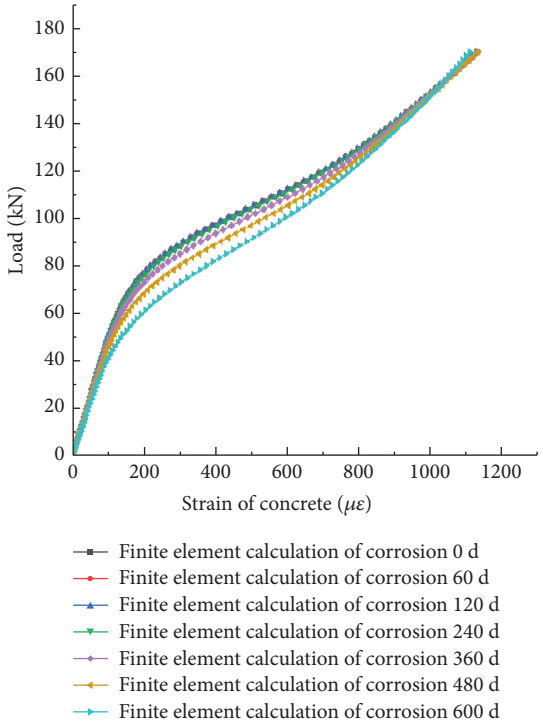

Figure 11: Load strain behavior of concrete at beam bottom.

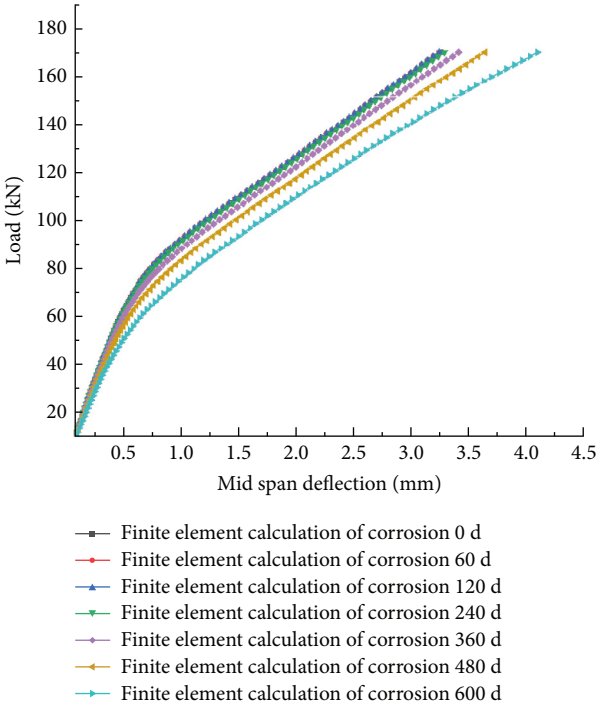

Figure 12: Load deflection curve.

right, indicating that under the condition that the test beam is subjected to the same size of the load, the higher the corrosion degree of the beam body, the smaller the stiffness and the worse the flexural mechanical performance, the greater the corresponding deflection, with the maximum increase of about 28%. Because the coincidence degree of the three curves of 0 d, 60 d, and 120 d is too high, it is difficult to distinguish the changes, so it is necessary to zoom in further. The results show that the corrosion curves of 60 d and 120 d are above the corrosion curve of 0 d, indicating that the deflection is smaller under the same load, indicating that the flexural mechanical properties of the test beam are improved in the corrosion time of 0~120 d. In conclusion, with the increase of sulfate corrosion time, the stiffness of the test beam first increases and then decreases; that is, with the

Table 4: Cracking load and flexural capacity corresponding to different corrosion days.

Corrosion days (d)	Cracking load (kN)	Flexural capacity (kN)
0	24.55	178
60	24.59	179.21
120	24.59	179.21
240	24.53	175.92
360	24.35	171.83
480	24.03	164.84
600	23.35	154.03

Note: the cracking load corresponding to corrosion 0 d in the table is 24.55 kN, which is close to the 24 kN obtained from the test; the cracking load corresponding to 60 days of corrosion is 24.59 kN, which is somewhat different from the 32 kN obtained from the test. It may be due to human factors, and there is an error in the observation of the first crack.

Table 5: Degradation of effective cross-sectional area of flexural section.

Corrosion time t (d)	Flexural capacity (kN)	Bending moment (kN·m)	Effective flexural cross-sectional area (mm^2)	Degradation of the effective cross-sectional area i (%)	Degradation rate of the effective cross-sectional area (10^{-5})
0	178	59.33	47600.00	0	—
240	175.92	58.64	47240.50	0.76	3.17
360	171.83	57.28	46761.17	1.76	8.33
480	164.84	54.95	45922.35	3.52	14.67
600	154.03	51.34	44604.20	6.29	23.08

Note: degradation rate of effective cross-sectional area = $(i_2 - i_1)/(t_2 - t_1)$.

deepening of corrosion, the flexural mechanical properties of the beam first increase and then decrease.

4.4.4. Effective Cross-Sectional Area of Bending Section of Test Beam. By analyzing the results of the ABAQUS finite element model, the cracking load of the test beam under different corrosion times can be obtained. According to the code, the theoretical flexural capacity of the section before corrosion of the test beam is 178 kN, and the corresponding deflection in the finite element model is 3.492 mm. Based on the deflection, the flexural capacity corresponding to each corrosion day can be obtained by applying displacement force. The results are shown in Table 4.

The change in the effective cross-sectional area of the flexural section is obtained according to the degradation of the flexural bearing capacity. Between 0 and 120 d of corrosion, the flexural mechanical properties of the test beam are improved due to the compactness of the concrete structure, so there is no degradation of the effective cross-sectional area of the flexural section. Therefore, from 240 d, the analysis results are shown in Table 5.

It can be seen from Table 5 that through analysis, it is found that with the change of corrosion time, the degradation rate of the effective cross-sectional area of sulfate corrosion test beam is 3.17, 8.33, 14.67, and 23.08, which increases exponentially. That is, the corrosion rate is faster and faster, the degradation degree of effective cross-sectional area is greater and greater, and the attenuation degree of the whole stiffness is stronger and stronger, which finally leads to the decreasing trend of beam bearing capacity. In the actual engineering analysis, the reason for the reduction of the effective cross-sectional area of the bending section is that after the sulfate corrodes the beam body, the part of the external concrete in contact with the corrosive environment is eroded, resulting in strength degradation, even cracking and spalling, reducing the effective cross-sectional area, deteriorating the stiffness of the beam body, and deteriorating the bearing capacity.

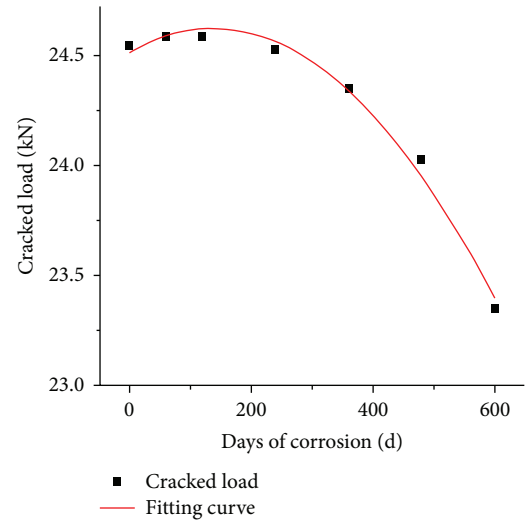

Figure 13: Fitting diagram of a variation of cracking load with sulfate corrosion time.

4.4.5. Calculation of Cracking Load and Flexural Capacity of Test Beam. It can be seen from Table 5 that with the increase of corrosion time, the cracking load increases first and then decreases. In order to better analyze the change of cracking load with corrosion time and study the change degree of mechanical properties of concrete beams under long-term

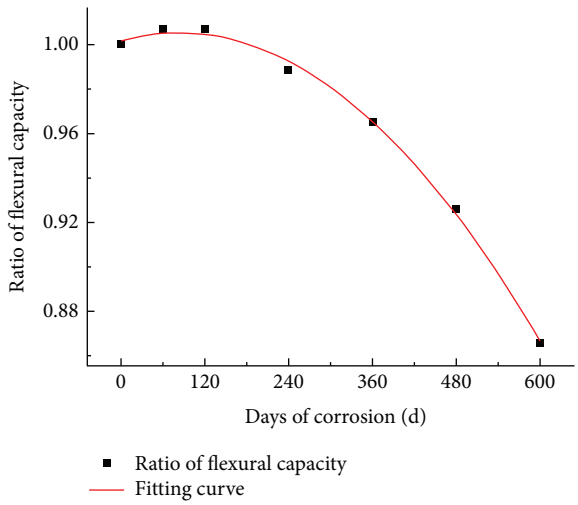

Figure 14: Fitting diagram of bending capacity with sulfate corrosion time.

sulfate corrosion, the quadratic polynomial can be used to fit the above results to obtain the calculation formula of formula (1), and the fitting curve is shown in Figure 13.

$$P_{cr} = 24.52 - 1.59 \times 10^{-3} t - 5.76 \times 10^{-6} t^2, \quad \text{correlation coefficient } R^2 = 0.986. \tag{3}$$

In addition, compared with that before corrosion, the flexural capacity increased by 0.68% at 60 d and 120 d and then showed a downward trend as a whole. It decreased by 1.17% at 240 d, 3.47% at 360 d, 7.39% at 480 d, and 13.47% at 600 d. It can be found that the decline rate of flexural capacity increased exponentially, indicating that the degradation rate of flexural mechanical properties of the test beam is faster and faster. Therefore, another percentage method can be used to reflect the degradation of bearing capacity; that is, the following formula can be obtained by fitting:

$$\frac{P_{ut}}{P_{u0}} = 1.002 + 8.559 \times 10^{-5} t - 5.180 \times 10^{-7} t^2, \quad \text{correlation coefficient } R^2 = 0.997, \tag{4}$$

where the flexural capacity of the test beam without p_{u0} corrosion, $p_{u0} = 178$ kN; and P_{ut} is the flexural capacity of the test beam corroded for t days. The fitting degree is good, and the fitting curve is shown in Figure 14.

5. Conclusion

In the early stage of corrosion, the strength of concrete increases. The main reason is that, in the early stage of corrosion, the expansive products generated by sulfate and concrete fill the pores of the structure, compact the concrete, and produce expansive internal stress, which improves the flexural mechanical properties of the structure to a certain extent. Comparing the test data with the finite element calculation results, it can be found that the calculation results obtained by ABAQUS finite element numerical simulation are in good agreement with the test data. Through the numerical simulation under different corrosion days, it is found that with the increase of sulfate corrosion time, the strength and stiffness of the beam have experienced a process of first increasing and then decreasing. It shows that sulfate corrosion does have a significant impact on the flexural mechanical properties of concrete, and the structural performance will deteriorate under long-term corrosion, which will affect the durability of the beam and reduce its service life. At the same time, the cracking load and flexural capacity also increase first and then decrease, which is consistent with the mechanism of sulfate compacting first and then deteriorating concrete structure. Therefore, the deterioration model of cracking load and flexural capacity with corrosion time is accurate through data fitting.

Sulfate corrosion is a complex and slow process with many influencing factors. This paper only studies 10% sodium sulfate solution. The concentration and type of sulfate have a profound impact on the test results. If magnesium sulfate solution is used, the test results may change greatly. Moreover, due to the time limit, only the mechanical properties of two beams corroded for 0 d and 60 d are studied, and the test data are very limited. Therefore, in future research, it is suggested to increase the corrosion days to 2 years or even 3 years, so as to obtain more data for more practical analysis and research.

Data Availability

The data generated or used during the study are included within the article.

Conflicts of Interest

The authors declare that they have no conflicts of interest.

Acknowledgments

This study was supported by the Science and Technology project of Gansu Provincial Department of Transportation (2020-05), Provincial Natural Science Foundation of Gansu Youth Fund (20JR5RA435), Gansu University Innovation Fund Project (2020A-026), Science and Technology Plan of Gansu Province (21JR7Ra306), and Hongliu Outstanding Young Talents Support Program of Lanzhou University of Technology (062006).

References

[1] D. Niu, *Durability and Life Prediction of concrete Structures*, Science Press, Beijing, China, 2003.

[2] J. Ran, *Study on the Influence of Cracks on the Durability of Bridge Structures in Northwest China*, Lanzhou Jiaotong University, Jiaotong, China, 2018.

[3] Y. Bao and J. Chen, "A new model of damage evolution of concrete under sulfate attack," *Journal of Ningbo University*

(Science and Engineering Edition), vol. 29, no. 1, pp. 98–102, 2016.

[4] L. Jiang, *Study on Deterioration Law of concrete under Sulfate Attack Environment*, Xi'an University of Architecture and Technology, Xi'an, China, 2014.

[5] L. Linlin, *Study on Corrosion of concrete by Sulfate and Inhibition Mechanism of Chloride under Different Mechanisms*, China University of Mining and Technology, Beijing, China, 2016.

[6] B. Bai, R. Zhou, G. Q. Cai, W. Hu, and G. C. Yang, "Coupled thermo-hydro-mechanical mechanism in view of the soil particle rearrangement of granular thermodynamics," *Computers and Geotechnics*, vol. 137, no. 8, Article ID 104272, 2021.

[7] B. Bai, Q. K. Nie, Y. K. Zhang, X. L. Wang, and W. Hu, "Cotransport of heavy metals and SiO2 particles at different temperatures by seepage," *Journal of Hydrology*, vol. 597, Article ID 125771, 2021.

[8] B. X. Yuan, Z. H. Li, Z. L. Su, Q. Z. Luo, M. J. Chen, and Z. Q. Zhao, "Sensitivity of multistage fill slope based on finite element model," *Advances in Civil Engineering*, vol. 2021, Article ID 6622936, 13 pages, 2021.

[9] L. Tao, Z. Sun, and K. Ding, "Research progress on mechanical properties and corrosion products of sulfate eroded concrete," *Concrete and Cement Products*, vol. 273, no. 1, pp. 1–5, 2019.

[10] Z. Jin, *Durability and Life Prediction of concrete under Severe Environment in Western China*, Southeast University, Dhaka, Bangladesh, 2006.

[11] C. D. Lawrence, "Mortar expansions due to delayed ettringite formation. Effects of curing period and temperature," *Cement and Concrete Research*, vol. 25, no. 4, pp. 903–914, 1995.

[12] O. S. B. Al-Amoudi, "Attack on plain and blended cements exposed to aggressive sulfate environments," *Cement and Concrete Composites*, vol. 24, no. 3-4, pp. 305–316, 2002.

[13] S. Chen and B. Wang, "Study on durability of bridge concrete structure under severe corrosion environment," *Journal of railway engineering*, vol. 35, no. 12, pp. 26–30, 2018.

[14] S. Zhang, *Sulfate Corrosion Mechanism of Concrete in Complex Environment*, Qingdao University of Technology, Qingdao, China, 2014.

[15] B. X. Yuan, Z. H. Li, Y. M. Chen et al., "Mechanical and microstructural properties of recycling granite residual soil reinforced with glass fiber and liquid-modified polyvinyl alcohol polymer," *Chemosphere*, vol. 268, Article ID 131652, 2021.

[16] B. Bai, D. Y. Rao, T. Chang, and Z. G. Guo, "A nonlinear attachment-detachment model with adsorption hysteresis for suspension-colloidal transport in porous media," *Journal of Hydrology*, vol. 578, Article ID 124080, 2019.

[17] A. Shishegaran, M. R. Khalili, B. Karami, T. Rabczuk, and A. Shishegaran, "Computational predictions for estimating the maximum deflection of reinforced concrete panels subjected to the blast load," *International Journal of Impact Engineering*, vol. 139, Article ID 103527, 2020.

[18] A. Shishegaran, M. R. Ghasemi, and H. Varaee, "Performance of a novel bent-up bars system not interacting with concrete," *Frontiers of Structural and Civil Engineering*, vol. 13, no. 6, pp. 1301–1315, 2019.

[19] A. Shishegaran, B. Karami, T. Rabczuk, A. Shishegaran, M. A. Naghsh, and M. Mohammad Khani, "Performance of fixed beam without interacting bars," *Frontiers of Structural and Civil Engineering*, vol. 14, no. 5, pp. 1180–1195, 2020.

[20] M. A. Naghsh, A. Shishegaran, B. Karami et al., "An innovative model for predicting the displacement and rotation of column-tree moment connection under fire," *Frontiers of Structural and Civil Engineering*, vol. 15, no. 1, pp. 194–212, 2021.

[21] B. Karami, A. Shishegaran, H. Taghavizade, and T. Rabczuk, "Presenting innovative ensemble model for prediction of the load carrying capacity of composite castellated steel beam under fire," *Structures*, vol. 33, pp. 4031–4052.

[22] A. Shishegaran, M. Saeedi, S. Mirvalad, and A. H. Korayem, "The mechanical strength of the artificial stones, containing the travertine wastes and sand," *Journal of Materials Research and Technology*, vol. 11, pp. 1688–1709, 2021.

[23] A. Shishegaran, B. Karami, E. S. Danalou, H. Varaee, and T. Rabczuk, "Computational predictions for predicting the performance of steel 1 panel shear wall under explosive loads," *Engineering Computations*, vol. 3, pp. 1–19, 2021.

[24] A. Shishegaran, H. Varaee, T. Rabczuk, and G. Shishegaran, "High correlated variables creator machine: prediction of the compressive strength of concrete," *Computers & Structures*, vol. 247, Article ID 106479, 2021.

[25] A. Shishegaran, F. Daneshpajoh, H. Taghavizade, and S. Mirvalad, "Developing conductive concrete containing wire rope and steel powder wastes for route deicing," *Construction and Building Materials*, vol. 232, Article ID 117184, 2020.

[26] J. Liu, S. Song, and M. Gao, "Study on the mechanism of carbon sulfur wollastonite formed by cement-based materials in corrosive environment," *Journal of Building Materials*, vol. 20, no. 6, pp. 846–853, 2017.

[27] A. Atkinson, D. J. Goult, and J. A. Heame, "An assessment of the long-term durability of concrete in radioactive waste repositories," *Materials Research Society*, vol. 50, 1985.

[28] D. Pan, *Research on Key Technologies to Improve the Durability of concrete Bridges in Alpine Areas*, Chongqing Jiaotong University, Shanghai, China, 2010.

[29] F. Zhang, Y. Yuan, and J. Du, "Study on damage detection of concrete members corroded by sulfate," *Journal of China University of Mining and Technology*, vol. 40, no. 3, pp. 373–378, 2011.

[30] Y. Tang, H. Lu, and Y. Zou, "Experimental study on flexural behavior of composite reinforced concrete beams," *Journal of Southeast University (Natural Science Edition)*, vol. 50, no. 05, pp. 822–830, 2020.

[31] F. Zhou, X. Wen, and D. Yunxing, "Flexural behavior of reinforced concrete beams strengthened with TRC plates," *Journal of Central South University*, vol. 49, no. 1, pp. 183–191, 2018.

[32] W. Liu, M. Xu, and Z. Chen, "Parameter calibration and verification of ABAQUS concrete damage plastic model," *Industrial Architecture*, vol. 44, no. S1, pp. 167–171, 2014.

[33] R. Gao, *Study on Micro Macro Deterioration Law of concrete Sulfate Erosion in Complex Environment*, Tsinghua University, Beijing, China, 2010.

[34] X. Wan, *Study on Diffusion Reaction Law and Numerical Simulation of concrete under Sulfate Attack Environment*, Nanjing University of Technology, Nanjing, China, 2010.

[35] Y. Liang and Y. Yuan, "Constitutive relation of concrete under uniaxial compression after sulfate corrosion," *Journal of Harbin Institute of Technology*, vol. 40, no. 4, pp. 532–535, 2008.

[36] G. Zhenhai and S. Xudong, *Principle and Analysis of Reinforced concrete*, Tsinghua University Press, Beijing, China, 2003.

[37] D. Niu, *Durability of Concrete in Complex Environment*, Science Press, Beijing, China, 2020.

[38] P. Zeng, *Finite Element Analysis and Application*, pp. 166–376, Tsinghua University Press, Beijing, China, 2004.
[39] P. Zhao, "Study on restoring force model of precast concrete frame beam column joints," *Earthquake Resistance and Reinforcement of Engineering*, vol. 38, no. 6, pp. 55–59, 2016.
[40] F. Wang, Z. Luo, and X. Lan, "Finite element analysis of axial compression performance of reinforced concrete beam column corner joints with built-in steel tube reinforced circular steel tube," *Journal of Building Structures*, vol. 36, no. S1, pp. 367–374, 2015.
[41] J. Jiang, F. He, and Y. He, *Finite Element Method and its Application*, pp. 54-55, China Machine Press, Beijing, China, 2006.